Rapid Ice Unloading in the Southern Antarctic Peninsula and its Effect on Bedrock Uplift Rates

Chen Zhao[1], Matt A. King[1], Christopher S. Watson[1], Valentina R. Barletta[2], Andrea Bordoni[3], Matthew Dell[1], Pippa L. Whitehouse[4]

[1] School of Land and Food, University of Tasmania, Australia; Chen.Zhao@utas.edu.au

[2] DTU Space, Technical University of Denmark, Kongens Lyngby, Denmark

[3] DTU Compute, Technical University of Denmark, Kongens Lyngby, Denmark

[4] Department of Geography, Durham University, United Kingdom

Abstract:

Rapid regional warming in the Antarctic Peninsula has led to the significant retreat and eventual collapse of several major ice shelves since the 1970s, triggering the subsequent acceleration and thinning of their feeding glaciers. The Wordie Ice Shelf, lying off the west coast of the Antarctic Peninsula, has undergone long-term disintegration since the 1960s with a substantial calving event occurring around 1989, followed by continuous steady retreat and its almost-complete disappearance. The dynamic response of the upstream glaciers to the ice shelf collapse and the response of the solid Earth to the associated mass loss are not fully understood. To quantify the mass loss from the system, we generated a digital elevation model (DEM) using airborne vertical and oblique imagery from 1966 and compared it to a DEM derived from 2008 SPOT data. This analysis reveals lowering over that time of approximately 60 m at the front of Fleming Glacier. Using IceBridge and ICESat-2/GLAS data spanning 2002-2014, we show an increased magnitude of mean elevation change rate, with rates post-2008 more than twice those of 2002-2008. We use these load change data as a basis for the simulation of viscoelastic solid Earth deformation. We subtract modelled elastic deformation rates, and a suite of modelled viscous rates, from GPS-derived three-dimensional bedrock velocities at sites to the south of Fleming Glacier to infer properties of Earth rheology. Assuming the pre-breakup bedrock uplift was positive due to post-Last Glacial Maximum (LGM) ice retreat, our viscoelastic-corrected GPS uplift rates suggest upper mantle viscosities are $> 2\times10^{19}$ Pa s and likely $>1\times10^{20}$ Pa s in this region, 1-2 orders of magnitude greater than previously found for the northern Antarctic Peninsula. Horizontal velocities at the GPS site nearest the Fleming Glacier, after the application of elastic and plate tectonic corrections, point away from Marguerite Bay rather than the present glacier front. This suggests that horizontal motion in the region reflects the earlier retreat of the glacier system following the LGM, compatible with a relatively strong mantle in this region. These findings highlight the need for improved understanding of ice load changes in this region through the late Holocene in order to accurately model glacial isostatic adjustment.

Keywords: Antarctic Peninsula, Wordie Ice Shelf, ice-mass loss, Glacial Isostatic Adjustment, GPS, upper mantle viscosity

1 Introduction

Rapid regional climate warming in the second half of the 20th Century, in both the atmosphere and ocean (Cook et al., 2016), led to the retreat and disintegration of major ice shelves across the Antarctic Peninsula (AP) and extensive changes in coastal tributary glaciers (Cook et al., 2005; Cook et al., 2016; Wendt et al., 2010; Wouters et al., 2015). In response to the loss of floating ice shelves and ice in fjords, outlet glaciers have exhibited acceleration and dynamic thinning (Rignot et al., 2004; Seehaus et al., 2016). A purely elastic response to unloading in the northern AP has been shown to be insufficient to explain the observed uplift pattern, while a rapid viscoelastic response (upper mantle viscosities (UMV) $<3\times10^{18}$ Pa s) demonstrates very good agreement with the observations (Nield et al., 2014; Thomas et al., 2011). Compared to the northern AP, the southern AP (Palmer Land) overall appears to have a significantly stronger rheology (UMV of $1\text{-}3\times10^{20}$ Pa s) (Argus et al., 2014; Ivins et al., 2013; Nield et al., 2012; Whitehouse et al., 2012a; Wolstencroft et al., 2015a), although the observed pattern of present-day deformation is yet to be fully explained by models – including an anomalous southward motion in northernmost Palmer Land (Wolstencroft et al., 2015a).

Wordie Ice Shelf (WIS) (Fig. 1) is one of seven AP ice shelves that collapsed in the last sixty years (Cook and Vaughan, 2010; Scambos et al., 2000). The WIS entered a period of sustained but intermittent retreat in the 1960s, and subsequently Fleming Glacier, its main tributary glacier, is observed to have accelerated and thinned through to end of 2008 (Rignot et al., 2005; Wendt et al., 2010). As such, the WIS system represents a very good example of long-term sustained dynamic thinning following the retreat/collapse of an Antarctic ice shelf.

In this paper we revisit the thinning of the glaciers feeding WIS, using airborne and satellite altimetry to quantify changes in ice elevation from 1966 through to early 2015 (hereafter ice elevation change is assumed to be equivalent to ice thickness change). We then consider the effect of the estimated high-resolution loading changes on the solid Earth, by considering models of elastic and viscoelastic deformation. In particular, we attempt to use observed responses to these relatively well-quantified ice load changes to constrain the solid Earth

rheology in this region. Furthermore, we test the hypothesis put forward by Wolstencroft et al. (2015a) that the anomalous southward motion of northern Palmer Land could be due to recent ice load changes in the WIS region.

2 Background

2.1 Changes in ice dynamics

The WIS lies off the west coast of the AP, in Marguerite Bay, and drains a grounded catchment of 15,000 km^2 (Vaughan, 1993). It is fed by seven glaciers (Figure 1), which can be divided into three main input units: Hariot glaciers in the north; Airy, Rotz, Seller, Fleming and Prospect in the middle; and Carlson in the south.

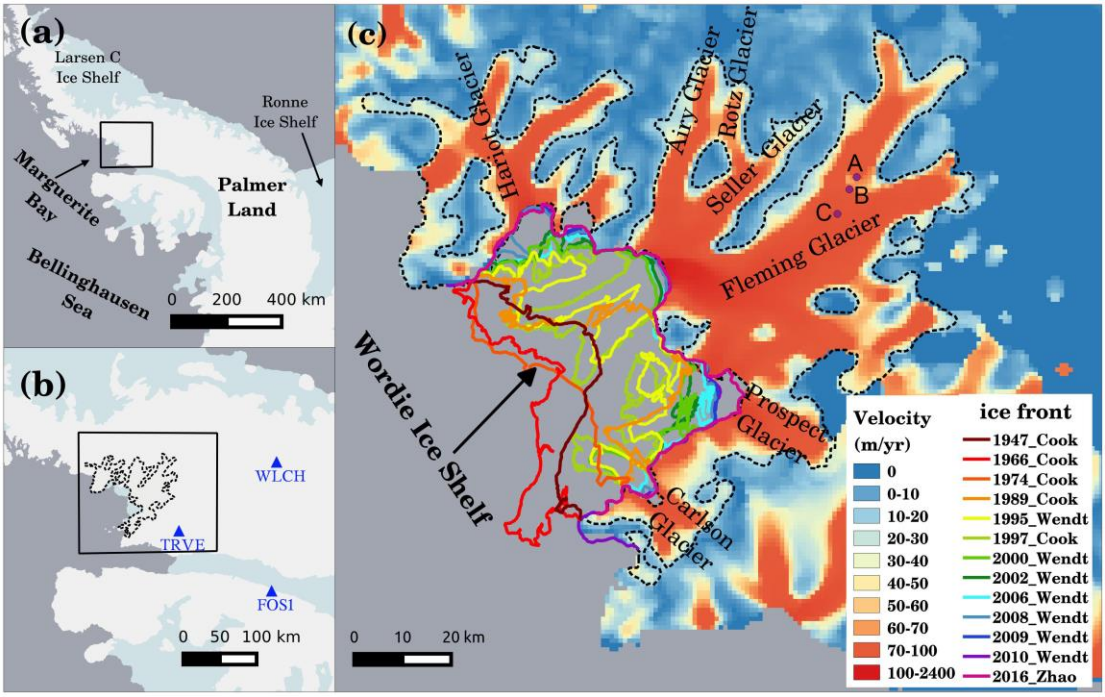

Figure 1 a) Location of Wordie Ice Shelf, Antarctic Peninsula. b) Three GPS sites near the Wordie Ice Shelf c) Ice front positions of Wordie Ice Shelf and its feeding glaciers. The shading relates to the observed ice velocity derived during austral summer 2007-2008 from Rignot et al. (2011b) and recorded ice shelf fronts are shown in colored lines (Cook and Vaughan, 2010; Wendt et al., 2010). The dotted black line is the boundary of ice velocity greater than 20 m/yr acquired from Rignot et al. (2011b) and the solid black line is the grounding line in 1996 from

Rignot et al. (2011a). Points A, B and C marked on Fleming Glacier relate to the locations for which velocity time series are available.

The WIS has undergone a series of calving events since the 1960s with a significant breakout between 1988 and 1989 as shown in Figure 1 (Cook and Vaughan, 2010; Doake and Vaughan, 1991; Rignot et al., 2005; Wendt et al., 2010). After this, the ice shelf area and front stabilized until around 1997 before gradually retreating back towards its present location (Cook et al., 2005; Doake and Vaughan, 1991; Wendt et al., 2010).

The temporal evolution of change is shown in Fig.2. We added an ice front position for February 2016, extracted from a Landsat 8 OLI_TIRS scene, revealing that the remaining ice shelf has an area of just 54 km^2 (using the 1996 grounding line from Rignot et al. (2011a)). The fronts of all glaciers now coincide with the 1996 grounding line except for Prospect Glacier, Carlson Glacier and an unnamed glacier next to Hariot Glacier (see the 2016 ice front in Fig. 1c).

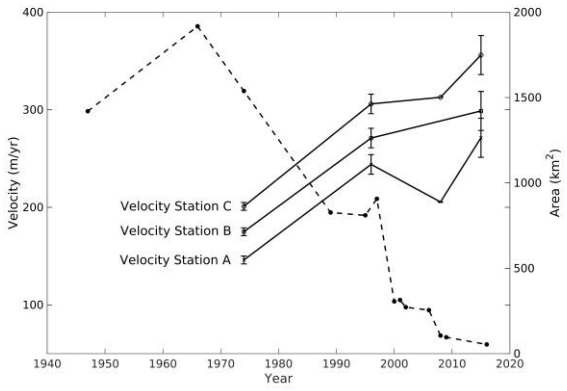

Figure 2 Time series of the Wordie Ice Shelf area (dashed line) compiled from different sources (Wendt et al. (2010), Cook and Vaughan (2010) and Landsat 8 OLI_TIRS data in Feb 2016) and of ice velocities at three locations (A, B, and C at Fig. 1c) in 1974 and 1996 from Doake (1975) and Rignot et al. (2005). The ice velocities at Station A and C in 2008 are from Wendt et al. (2010) and in 2015 were derived from Landsat 8 data (Gardner et al., 2017).

Likely as a result of the collapse of the ice shelf, the feeding glaciers of the WIS accelerated and have been rapidly thinning and losing mass into the ocean. The velocity of the upstream

region of Fleming Glacier (locations A, B and C on Fig. 1c) increased by 40-50% between 1974 and 1996, remained largely unchanged in 2008 (Fig. 2) (Doake, 1975; Rignot et al., 2005; Wendt et al., 2010), but increased sharply again between 2008 and 2015 despite almost no ice shelf remaining in front of Fleming Glacier since 2008. Detailed elevation change data have been published for the period 2004-2008 over Fleming Glacier and show the greatest change at its downstream extent with lowering of up to 4.1 ± 0.2 m/yr between December 2004 and December 2008 (Wendt et al., 2010).

2.2 Glacial Isostatic Adjustment

Due to the demise of the major ice sheets following the Last Glacial Maximum (LGM), ice-ocean surface loads on the solid Earth have been redistributed, reshaping Earth's gravitational field, altering the orientation of its rotation pole, and causing viscoelastic deformation of the solid Earth (Peltier, 2004); these processes are collectively known as glacial isostatic adjustment (GIA). Inputs required in a GIA model include the rheology of the Earth and the spatiotemporal evolution of ice-loading, enabling the prediction of three-dimensional solid earth deformation and geoid rate change (King, 2013; Peltier et al., 2015; Whitehouse et al., 2012a).

Conventional models of Antarctic GIA consider only millennial-scale loading changes following the LGM, and they often assume that deglaciation was complete several thousand years before present, e.g. Argus et al. (2014); Ivins et al. (2013); Whitehouse et al. (2012a). As such, any loading changes since that time are not accounted for, although the relatively high upper mantle viscosities employed in such models (5×10^{20} Pa s in ICE-6G_C (Argus et al., 2014), 2×10^{20} Pa s in IJ05_R2 (Ivins et al., 2013), and 1×10^{21} Pa s in W12 (Whitehouse et al., 2012b)) mean that small load changes during the last few thousand years would have little impact on the present-day deformation pattern. This is not the case, however, if mantle viscosities are lower than 10^{20} Pa s (Ivins et al., 2000). Indeed, the viscoelastic deformation of the AP due to recent (centennial to decadal) ice load changes has been the subject of several recent studies (Nield et al., 2014; Nield et al., 2012; Wolstencroft et al., 2015a). For example,

Nield et al. (2014) found it necessary to invoke mantle viscosities of 6×10^{17} - 2×10^{18} Pa s to explain the rapid uplift of the northern AP following the breakup of the Larsen B Ice Shelf in 2002. Focusing on the southern limit of the AP, Wolstencroft et al. (2015a) found they could not explain the spatial pattern of uplift observed by GPS after correction for elastic deformation, and concluded that poorly known late Holocene (last few thousand years) loading changes may be responsible, implying that mantle viscosities are sufficiently low to allow for deformation over this timescale.

While did not extensively consider horizontal GPS velocities, they noted that the southward motion of GPS site TRVE (Fig. 1b) was anomalous to the pattern of deformation recorded at the other sites. Southward motion at TRVE would be consistent with late Holocene ice unloading in the Marguerite Bay region, which would be sufficiently distant that it would not affect other GPS sites in the region, but the timing of this unloading is poorly known. Millennial-scale GIA models simply assume that the grounding line had retreated back to approximately the present location by ~5 calibrated thousand years (cal ka) before present (BP) based on the radiocarbon dates from marine sediment cores (Bentley et al., 2011; Ó Cofaigh et al., 2014; Whitehouse et al., 2012b), and they do not account for any recent changes associated with the WIS retreat, some of which are poorly understood.

As described above, ice load changes during the last 20 years are well documented but the full loading history since the commencement of retreat in the 1960s is not known, and consequently neither is the solid Earth's response. We next describe new datasets that help constrain the loading changes in this region.

3 Data and Methods

3.1 Ice unloading history

3.1.1 Altimetry data during 2002-2015

We assembled elevation measurements from Operation IceBridge and pre-IceBridge campaigns (2002, 2004, 2008-2011, 2014) (Krabill, 2014, updated 2016), and Geoscience

Laser Altimeter System/Ice, Cloud, and land Elevation Satellite (GLAS/ICESat, Feb 2003 to Oct 2009) (Zwally et al., 2014). From these we determined elevation change rates (dh/dt), fitting a linear regression to all measurements in each cell of a regular 250 m grid that has at least 3 measurement points (See Sec. S1 in the Supplementary Material (SM)). Here we limit our dh/dt analysis to regions with velocity greater than 20 m/yr (Rignot et al. (2011b), dotted line in Figs. 1b, 1c). The dh/dt showed clear correlation with absolute elevation (Figs 3c, 3d).

For our loading computations we need complete coverage of the three main feeding glacier regions and we computed this based on the observed dh/dt and glacier hypsometry. We evaluated the fit of the hypsometric model to the data for chosen grid cells using a weighted root mean square error (RMSE), and the RMSE is 0.89 m/yr and 0.20 m/yr pre- and post-2008, respectively (see Fig. 3 and Sec. S1 in the SM).

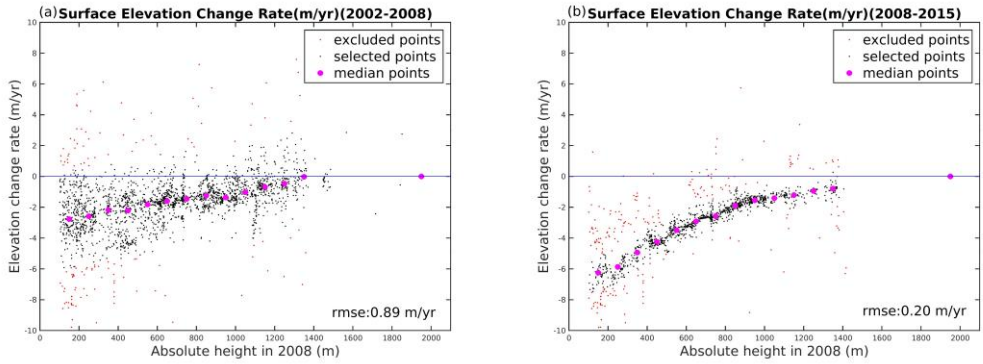

Figure 3. Elevation change rates (black dots) a) over 2002-2008 and b) over 2008-2015 against absolute surface height in 2008. The magenta dots are the median values for each 100 m height bin.

To compare our dh/dt values with those previously published using the ATM data from 2004 and 2008 only (Wendt et al., 2010) we computed dh/dt for three different periods (2002-2004, 2004-2008 and 2008-2015). Aside from Fleming Glacier, Prospect Glacier, Airy Glacier, Rotz Glacier, and Seller Glacier, where the majority of the airborne data focus (referred to hereafter as the Fleming system), we also made use of data from the other two main feeding regions (Hariot Glacier and Carlson Glacier; referred to hereafter as the HC system). We found that dh/dt values across the Fleming system did not change much over 2002 to 2008, but their magnitude increased markedly after 2008, coinciding with an increase in ice velocity (Fig. 2)

suggesting this is a result of dynamic mass loss. While data coverage for the HC system is spatially sparse, the rate of lowering appears to have remained stable from 2002 to 2015. So, for the loading deformation calculations below, we assumed that the surface lowering rate of Fleming system remained constant during 2002-2008 (Fig. 4a) and 2008-2015 (Fig. 4b), and that dh/dt values across the HC system did not change over the whole time period (that is, the rates in Fig 4a were used). The interpolated surface lowering rates at the front of Fleming Glacier (computed at elevation 150 m) are 2.77±0.89 m/yr during 2002-2008 and 6.25±0.20 m/yr during 2008-2015, respectively.

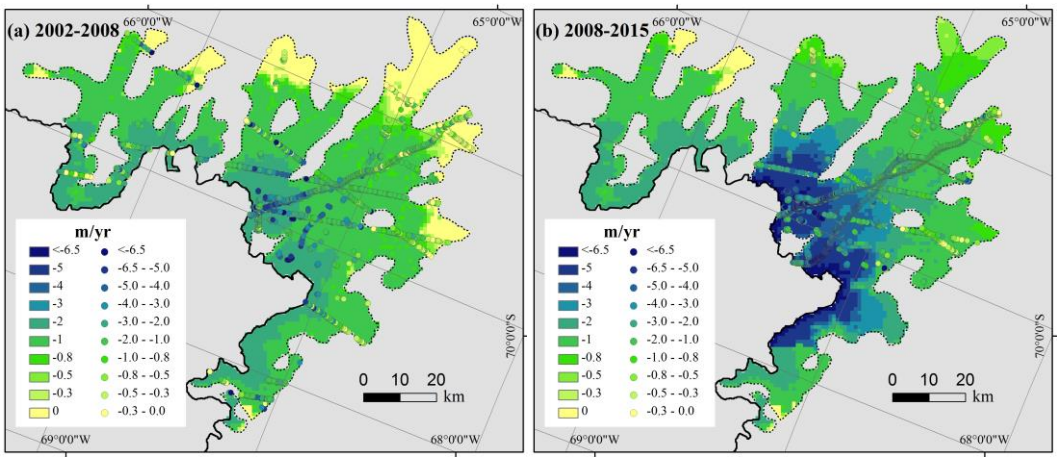

Figure 4. The distribution of dh/dt during a) 2002-2008 and b) 2008-2015 (colors) as derived from the hypsometric model based on the altimetry dh/dt (colored circles). The elevation change rate of the Hariot Glacier and Carlson Glacier system are identical in both panels. The maps cover the same region as Fig. 1c.

To estimate mass change over the entire region, we created a digital elevation model (DEM; WGS84 ellipsoid) of the feeding glaciers by merging an ASTER 100 m DEM product (Cook et al., 2012) with the SPIRIT 40 m DEM from SPOT 5 (Korona et al., 2009), and then resampled the merged product to 1000 m resolution. Using this DEM, the distribution of dh/dt for all feeding glaciers was determined via linear interpolation of the hypsometric model (Fig. 3). The results are shown in Figs. 4a and b.

3.1.2 Elevation changes during 1966-2008

To understand the elevation change pattern before 2002, we generated a DEM for 1966 using historic aerial photographs from November 1966 taken as part of the historical mapping campaigns. The 1966 DEM was then registered to the 2008 SPOT DEM (Korona et al., 2009) to estimate the elevation changes during 1966-2008 (See Sec. S2 in the SM). Differencing the co-registered DEMs provided estimates of surface elevation change. Median surface lowering near the front of Fleming Glacier was nearly 60 m (taken along two ice flow lines and three transverse lines parallel to the grounding line in the very front of Fleming Glacier; see Fig. 5) between 1966 and 2008 (nearly 41 years), equivalent to a mean surface lowering rate of 1.5 m/yr. A region upstream of the grounding line shows a total lowering of 80-100 m between 1966 and 2008 (see Fig. 5); we return to the implications of using a different surface lowering value in the discussion.

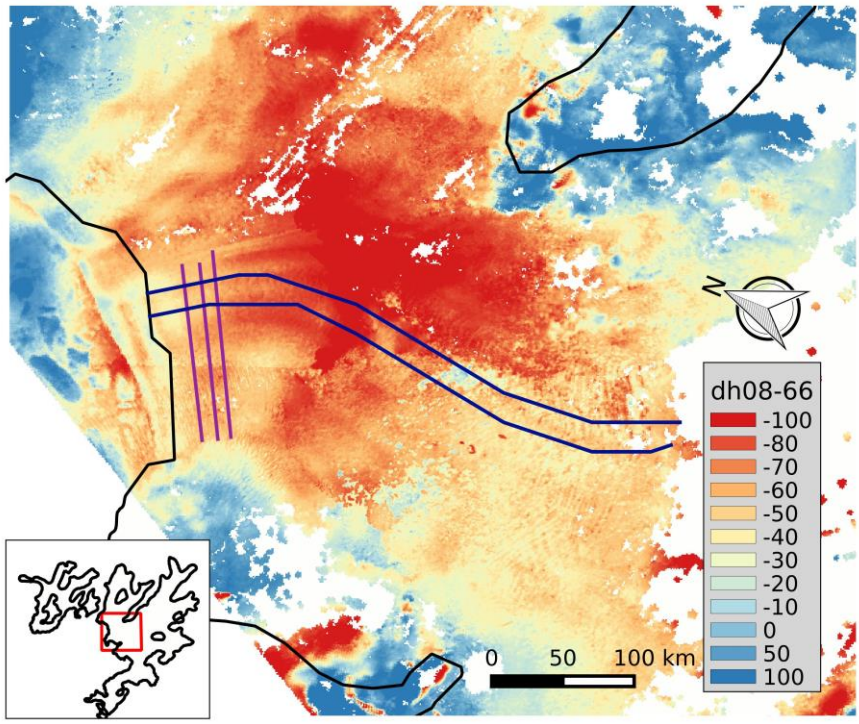

Figure 5. Elevation changes over 1966-2008. Black lines indicate the boundary of feeding glaciers with velocity > 20 m/yr. Blue and purple lines are the ice flow lines and the sampling lines used to compute the median of elevation change at the front of the Fleming Glacier, respectively. Inset map of the feeding glaciers shows the location of DEM data in 1966 (red box). The inset map covers the same region as Fig. 1c.

3.1.3 Temporal interpolation of changes prior to 2002

To simulate the viscoelastic response of the solid Earth to ice mass change we need an ice loading history. The elastic component (which must be accounted for within the GPS measurements) depends on contemporaneous ice load changes, while the viscous response also depends on past ice load changes. The extent of the time span to be considered depends largely on the mantle viscosity, however, which is unknown.

We start by assuming that the glacier system was stable before 1966. This assumption is supported by the small net change in the ice front position from 1947 to 1966 (Fig. 1c), but the precise evolution of the glacier system prior to the velocity observation in 1996 (Rignot et al., 2005), and near-continuous elevation measurements from 2002, is uncertain. To begin with, we assume that the lowering rate for 1996-2002 is the same as for 2002-2008, based on the observation of similar velocities over these two periods (Fig. 2).

In Sec. 3.1.2, we determined that the mean surface-lowering rate over 1966-2008 was 1.5 m/yr at the glacier front. We now determine the surface lowering rate for different epochs within this period: the surface-lowering rate from 2002 to 2008 in the same way (see Fig. 5) was approximately 2.5 m/yr (Fig. 4a). Therefore, the ice thinned by 15 m during 2002-2008 or equivalently 30 m during 1996-2008. This implies that lowering between 1966 and 1996 must have been ~30 m (or at a mean rate of 1 m/yr). In the absence of further information, we developed two plausible end member scenarios for the period 1966 to 1996, each with a total thinning of the ice front of 30 m (~ 1 m/yr on average). The scenarios are illustrated in Fig. S1 in terms of dh/dt, normalized to the values for 1996-2008. Scenario 1: As one end member we assume that the retreat of WIS in the 1960s substantially perturbed the back-stress on the grounded ice and hence resulted in a near-instantaneous increase in ice velocities (as observed for the Larsen B tributary glaciers, e.g. Rignot et al. (2004)). We assume that the increase in ice velocities resulted in a constant surface-lowering rate of 1 m/yr, which persisted until 1996. Between 1996 and 2008 a higher rate of surface lowering was assumed. Scenario 2: As the other end member, we assume that the glaciers gradually increased in velocity from 1966 to

241 1996 as a result of a gradual reduction in back-stress as the ice shelf thinned and retreated.
242 Using our constraint on total surface lowering from 1966 to 1996, the magnitude of dh/dt is
243 uniformly increased 5 times over this period.

244 As described in Sec. 3.1.1, the Fleming system has different surface lowering rates over the
245 periods 2002-2008 and 2008-2015, while the HC system maintained a constant thinning rate
246 during 2002-2015. For both glacier systems, we presume that the spatial pattern of elevation
247 change prior to 2002 was consistent with that over 2002-2008. To generate the spatial field of
248 change for earlier periods, we scale the map of 2002-2008 elevation changes.

249 For the loading computations, we convert from elevation change rate to mass change rate
250 (dm/dt) by accounting for modelled firn compaction and surface mass balance (SMB)
251 anomalies (see Sec. S3 in SM).

252 3.1.4 Far-field loading changes

253 For the far-field loading changes in Antarctica we adopt an approach and datasets similar to
254 Wolstencroft et al. (2015a). That is, we used ice mass trends for the northern AP (2002-2006,
255 2006-2011) obtained from Nield et al. (2014), a 5 km gridded ice load history for the southern
256 AP and Alexander Island (Nov. 2010-Sep. 2013) derived from CryoSat-2 data by McMillan et
257 al. (2014), and detailed mass change in the southern AP based on ICESat data from 2003 to
258 2009 acquired by Gunter et al. (2014) (see Table 2). For the post-2008 period, we assume that
259 ice mass change rates have remained constant since the latest observation in the northern AP,
260 southern AP and the Alexander Island. We modified the above to exclude data points inside the
261 feeding glacier system of the WIS, noting that the uncertainty of CryoSat-2 dh/dt data in this
262 region, as used by Wolstencroft et al. (2015a), is greater than 0.65 m/yr.

263 3.2 GPS

264 Three continuous GPS (cGPS) stations are located within ~200 km of Fleming Glacier, namely
265 TRVE, FOS1, and WLCH, with their locations shown in Fig. 1b (blue triangles) and Table 1.
266 We focus on these sites as they are the most sensitive to ice load changes in the feeding glaciers
267 of the WIS. All of them were installed during the 2009-10 Austral summer (Wolstencroft et al.,

2015a). FOS1 also has three occupations prior to 2009, in 1995, 1996 and 1998. The same sites were used by Wolstencroft et al. (2015a) although our analysis makes use of more recent data (Table 1). GPS data were analyzed as described in Wolstencroft et al. (2015a), removing the effect of atmospheric loading displacements in post-processing (Petrov, 2015); such a correction is particularly important for Antarctic time series (Santamaría-Gómez and Mémin, 2015).

Time series at FOS1 have offsets evident in at least the vertical component prior to 2009, presumably due to the changes in equipment that occurred during site occupations. As it is not possible to robustly model these offsets in our analysis, together with the limited data before 2009, we do not consider the early parts of the record from FOS1.

Before considering the horizontal time series further, we removed the effects of plate rotation using the plate rotation of Argus et al. (2014). As noted by Wolstencroft et al. (2015a) there is uncertainty in removing plate rotations from Antarctic GPS data which expresses as a bias in the residual horizontal velocities (see also (King and Santamaría-Gómez, 2016a-a); King et al. (2016b)); we consider this issue further below. We estimate site velocities from 2009 to 2015 using CATS software (Williams, 2008) at the same time as annual and semi-annual terms and assuming a white-plus-flicker noise model. The resulting velocities and uncertainties are shown in Table 1.

Table 1 GPS site names, locations, velocities, uncertainties, corresponding elastic correction, and modelled three-dimensional deformation from ICE-6G (VM5a) and W12. The horizontal components have been corrected for plate rotation using the Euler pole and rate from Argus et al. (2014): 59.876°S, −127.277°E and 0.2178 (deg/Ma). Uncertainties are one standard deviation (68% confidence intervals). The ICE-6G rates were interpolated from 1 degree grids whereas the W12 estimates are directly computed at the sites with the best fitting Earth model for the West Antarctic sites described in Whitehouse et al. (2012a), and are taken from Wolstencroft et al. (2015a).

Site	Lat	Lon	GPS collection (yyyymmdd)	Vertical rate (mm/yr)	Vertical uncertainty σ_V	Horizontal velocities after plate rotation	Horizontal uncertainty (mm/yr)	Elastic correction (mm/yr)	ICE-6G (mm/yr)	W12 1D (mm/yr)

						(mm/yr)	correction (mm/yr)												
			Start	End			North	East	σ_N	σ_E	Vert.	North	East	Vert.	North	East	Vert.	North	East
FOS1	-71.31	-68.32	20091218	20150210	1.63	0.90	0.57	0.52	0.30	0.26	1.84	-0.11	0.15	3.99	-0.77	0.16	6.46	0.82	0.34
TRVE	-69.99	-67.55	20091222	20141025	3.68	0.68	-1.62	0.01	0.30	0.29	3.42	-0.68	-0.13	3.64	-0.74	-0.02	5.98	0.92	0.15
WLCH	-70.73	-63.82	20100315	20151102	1.02	0.73	0.06	-0.08	0.26	0.32	1.38	-0.18	0.38	3.80	-0.52	0.24	4.64	0.69	0.61

3.3 Viscoelastic Modelling

3.3.1 Elastic modelling

For the elastic modelling we follow the approach previously used by Nield et al. (2014) and Wolstencroft et al. (2015a). That is, we used the elastic output of the VE-HresV2 (Visco-Elastic High Resolution technique for Earth deformations) code (Barletta et al., 2006). The load Love numbers were computed to a maximum spherical harmonic degree of 3700 based on a compressible, self-gravitating Earth using VE-CL0V3RS v1.4 (Visco-Elastic Compressible LOVe numbER Solver) with a PREM structure (Dziewonski and Anderson, 1981). We use the load Love numbers to compute Green's functions, which are spatially convolved with ice loading discs according to the methods presented in Barletta et al. (2006). The ice history, described in Sec. 3.1, is converted from ice elevation change to mass change for the feeding glaciers of the WIS, and as described in Wolstencroft et al. (2015a) for other regions.

Ice load changes across Alexander Island are not known before 2008, so we tested the sensitivity of our modelled displacements at TRVE and FOS1 to assumptions of either no ice load change over Alexander Island before 2008 or a constant rate of ice mass change during the whole period 2002 to 2015. The results revealed small differences (0.29 and 0.25 mm/yr for vertical rate difference, 0.09 and 0.09 mm/yr for horizontal rate difference at FOS1 and TRVE respectively, smaller than the GPS uncertainty), and hence we regard ice load change across Alexander Island to be negligible during 2002-2008.

We assumed negligible changes in ice load prior to 2002 in any region except for the feeding glaciers of WIS, and adopted a constant rate of mass change extending from the most recent data period to the present-day (e.g., 2011-2015 for the northern AP, and 2010-2015 for Alexander Island and southern AP; see Table 2). Changes in the far northern AP related to the

mid-1990s breakups of the Larsen A and Prince Gustav ice shelves will not be of significant consequence here due to the weak rheology in that region (Nield et al., 2014) .

Table 2 Data source of ice load changes (dm/dt) before and after 2008 on the feeding glaciers of the Wordie Ice Shelf (Fleming Glacier and Prospect Glacier, referred to as FGL, and other neighboring glaciers, referred to as OGL), the northern Antarctic Peninsula (NAP), Alexander Island (AI), and the southern Antarctic Peninsula (SAP).

Region	dm/dt (2002 -2008)		dm/dt (2008-2015)	
	Source	Time period	Source	Time period
FGL OGL				
NAP	Nield et al. (2014)	2002-2006	Nield et al. (2014)	2007-2011; extrapolated at the same rate to 2015
AI	No data		CryoSat-2 from McMillan et al. (2014)	2010-2013; extrapolated at the same rate to 2015
SAP	ICESat from Gunter et al. (2014)	2003-2009	CryoSat-2 from McMillan et al. (2014)	2010-2013; extrapolated at the same rate to 2015

3.3.2 Viscous modelling

We again follow Nield et al. (2014) in constructing a model of the Earth's viscous response to ice load changes, adopting a 4-layer model with a purely elastic lithosphere underlain by three distinct viscous layers with linear Maxwell rheology. We use the time-dependent viscous load Love numbers generated (with the code VE-CL0V3RS v1.4) for Nield et al. (2014), which were explicitly computed at sufficient epochs to allow interpolation (where necessary) with <10% error. The maximum spherical harmonic degree is 1195, which is sufficient for the spatial and temporal scale of the viscous response considered here.

The viscosity or thickness of the various layers is not well constrained in this region. In the northern AP, Nield et al. (2014) found a preferred model with lithospheric thickness (LT) 100 -140 km and upper mantle viscosity (UMV) between 6×10^{17} Pa s and 2×10^{18} Pa s. In the far south of the AP, Wolstencroft et al. (2015a) found a best-fit model with LT 120 km and a higher UMV of 1-3 $\times 10^{20}$ Pa s. We test a wide range of values for the Earth model, adopting an elastic lithosphere in the range 20 km to 130 km, a viscoelastic upper mantle of 400 km with viscosity between 1×10^{17} Pa s and 3×10^{20} Pa s, a fixed viscosity transition zone with a

base at 670 km and viscosity of 4×10^{20} Pa s, and a lower mantle with a viscosity of 1×10^{22} Pa s. Using even higher UMV would result in an elastic-only response over this time-period.

To compute the time series of modeled viscous deformation for each candidate Earth model at each GPS site, we convolved the viscous Love numbers with each of the two scenarios for ice loading history. We use the same load change datasets as in the elastic modelling. For the tests that follow, we primarily adopt Scenario 2, but also discuss the effect of adopting Scenario 1.

3.4 GIA modelling

The above modelling only considers decadal-scale load changes, while our GPS velocities could be sensitive also to any ongoing deformation related to earlier (centennial- or millennial-scale) GIA signal. To explore the direction and magnitude of this, we consider the output of two millennial-scale GIA models: the ICE-6G_C (Argus et al., 2014; Peltier et al., 2015) and W12 models (Whitehouse et al., 2012b), the latter was computed using both 1-D and 3-D Earth rheologies as described in King et al. (2016b). Predicted uplift rates at the GPS sites from the ICE-6G_C and W12 1D models are listed in Table 1.

4. GPS results

The GPS horizontal and vertical velocities of TRVE, FOS1 and WLCH are presented in Table 1 and Fig. 6 after correction for plate rotation and elastic effects. Our GPS velocities for these sites are slightly different to those of Wolstencroft et al. (2015a) due to our longer data period and an improved dataset for the elastic correction. Our higher-resolution ice loading data for Fleming Glacier produced a slightly greater elastic correction at the TRVE and WLCH sites as a result of a greater ice mass loss than that derived using CyroSat-2 data post-2010.

Fig. 6b shows that the modelled horizontal elastic deformation vector at TRVE (red dotted arrow) points away from Fleming Glacier as a result of the large center of ice mass loss at that location. However, unlike the Wolstencroft et al. (2015a) horizontal vector after plate rotation correction and elastic correction, our GPS analysis results in a corrected horizontal vector at TRVE that points away from the center of Marguerite Bay (red arrow in Fig. 6b). If viscous

deformation in this region were dominated by decadal-scale mass loss from the Fleming Glacier system, the vector would be expected to point away from the glacier (red dots in Fig. 6b). Instead, our data suggests that viscous deformation in the region does not just reflect the response to ice mass loss in the Fleming Glacier system, but also the effect of earlier ice load changes in Marguerite Bay since the LGM. Adopting an alternative model of plate rotation (Altamimi et al., 2011) would result in a TRVE horizontal vector that points even further into Marguerite Bay. The potential for biases in these derived plate rotation estimates (King and Santamaría-Gómez, 2016a-b; King et al., 2016b) means this conclusion is not definitive, however, and we explore the rheology further below. Unfortunately, FOS1 and WLCH are too far away for their horizontal velocities to provide useful information as to the distribution of ice mass change in the Fleming Glacier/Marguerite Bay region.

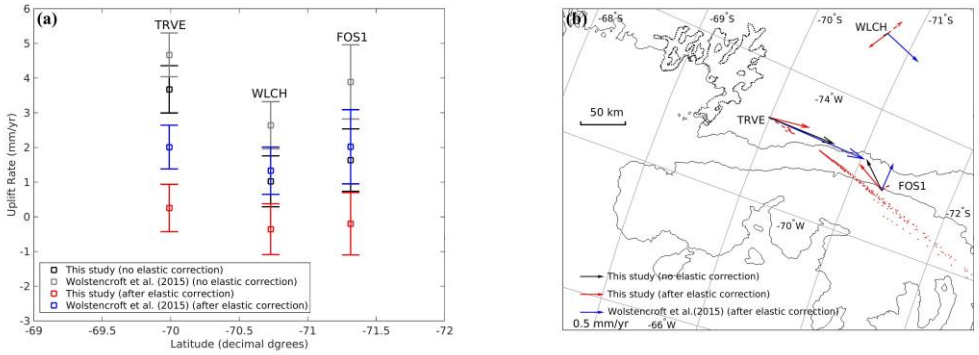

Figure 6. a) Observed GPS uplift rates without elastic correction from this study (dark gray) and Wolstencroft et al. (2015a) (light gray), and observed GPS uplift rates after elastic correction from this study (red) and as published by Wolstencroft et al. (2015a) (blue). b) Map view of observed GPS horizontal deformation rates at three sites. The black solid arrow shows the original measured horizontal rates after plate rotation correction. The red and blue solid arrows represent the horizontal rates after plate rotation correction and elastic correction from this study and as published by Wolstencroft et al. (2015a), respectively. The red dashed arrow displays the elastic correction component from this study. The red dots show the end of predicted viscoelastic deformation arrow at TRVE from the range of models in this study, considering post-1966 loading changes only.

5 Model fit analysis

We compared the GPS data with results from the various combined viscoelastic models, and calculated the misfit in both the vertical and horizontal directions. In the tests below we make use of the Scenario 2 loading history (Fig. S1b), but we also refer to scenario 1 for comparative purposes.

5.1 Viscoelastic modelling constrained by GPS vertical velocities

Firstly, we estimated the background (pre-1966) vertical velocity by computing the difference between observed and predicted uplift rates at TRVE, WLCH, and FOS1. We assume this background velocity is dominated by ice load changes from earlier time periods. This assumption is supported by predictions from both the ICE-6G_C and W12 1D models, which suggested positive uplift rates at the three GPS sites (Table 1) as a result of millennial-scale deglaciation. Ongoing uplift through to the late Holocene is also supported by evidence for relative sea level fall in Marguerite Bay over this period (Simkins et al., 2013).

On this basis, we test the adequacy of the viscoelastic models by assuming that the background rate of bedrock uplift in this region must be either close to zero or positive. Fig. 7a shows that background rates at TRVE are only close to zero or positive when upper mantle viscosities are greater than about 1×10^{20} Pa s. In contrast, there is little sensitivity to choices of LT at this site. Consideration of the uncertainty in the GPS velocity (σ_V in Table 1) would allow for only a slightly smaller lower limit to the UMV (2×10^{19} Pa s) (Fig. 7a).

The same comparisons at FOS1 and WLCH reveal a generally lower sensitivity to choice of Earth model due to their location farther away from Fleming Glacier. Considering them separately to TRVE, they allow for a relatively lower viscosity and thinner lithosphere (Figs. 7b and 7c), although viscosities lower than about 1×10^{18} Pa s are still excluded for most lithospheric thicknesses. Considering all sites together suggests a lower bound for the UMV of around 1×10^{20} Pa s, which is substantially larger than the value preferred for the northern AP

(Nield et al. (2014); red star in Fig. 7a) and consistent with the models for the whole of Palmer Land proposed by Wolstencroft et al. (2015a) (cyan star in Fig. 7a).

We repeated the above analysis, which was based on Scenario 2 (S2; Fig. S1b), but using Scenario 1, and reached very similar conclusions regarding the preferred Earth model (Fig. S4). That is, our finding that UMV in this region is greater than 1×10^{20} Pa s is not strongly sensitive to the timing of recent ice load changes.

We also explored the effect of making different assumptions when constructing our load change dataset (see Sec. S3 in SM). All of these tests suggest an UMV greater than around 2×10^{19} Pa s, and we suggest this is a robust lower bound for our Earth model. This bound is consistent with the preferred model of Wolstencroft et al. (2015a).

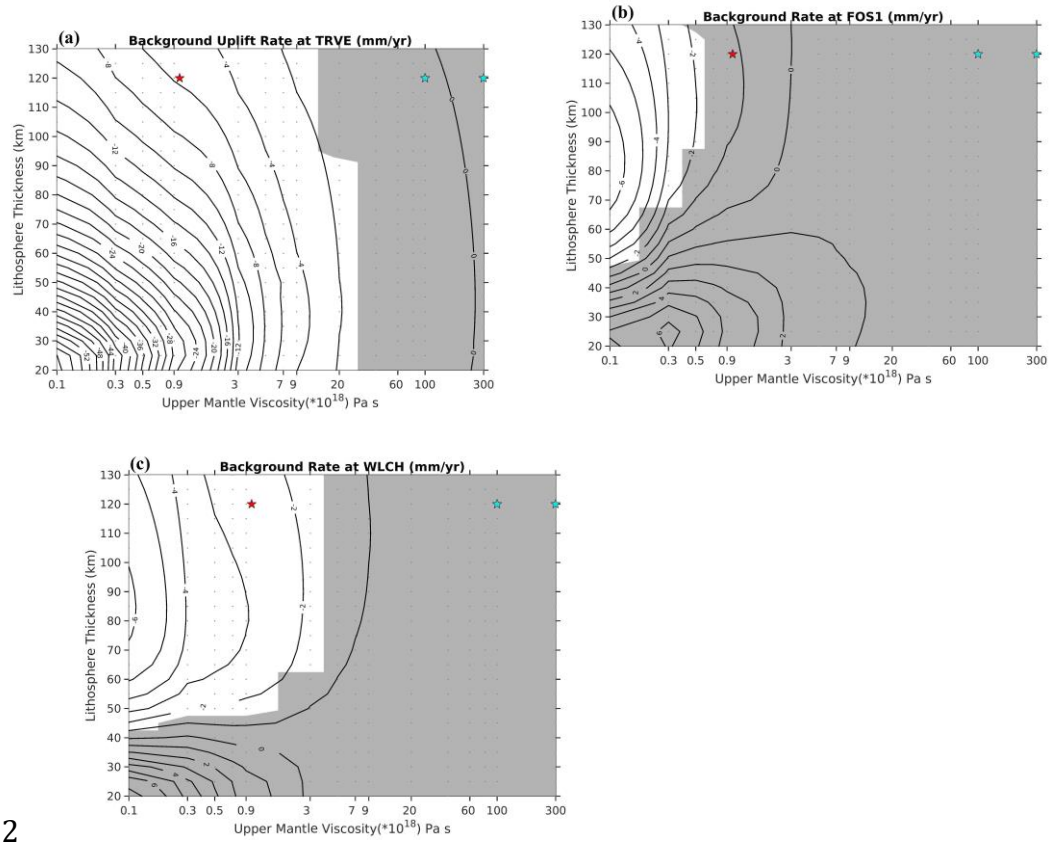

Figure 7. Estimated pre-1966 background uplift rates as a function of viscoelastic model setup at a) TRVE, b) FOS1 and c) WLCH. The red star is the best fit model for the northern AP from Nield et al. (2014), and the cyan stars span the range of upper mantle viscosities preferred by Wolstencroft et al. (2015a). The black lines are contours of the implied vertical background

rate. The gray shading areas indicate the Earth models with background rate greater than or equal to zero while considering measurement uncertainty (i.e., > $-2\sigma_V$).

5.2 Viscoelastic modelling constrained by GPS horizontal velocities

We next evaluated the different models by considering their ability to explain the observed horizontal velocities. We assume that the remaining signal after plate rotation correction can be explained by a sum of the decadal-scale viscoelastic deformation and that from late Holocene or earlier GIA (Argus et al., 2014). For simplicity, we extract a single rate of decadal-scale deformation at 2012.0 from each model. In the absence of late Holocene load data, we limit ourselves to exploring the general magnitude and direction of deformation predicted by millennial-scale GIA models. We considered predictions from ICE-6G_C, W12 1D, and another eight W12 models that were combined with 3D power-law viscosity models; these vary as a function of mantle grain size, water content and seismic model, as described by King et al. (2016b). We note that even in the presence of an UMV as low as 2×10^{19} Pa s, with a relaxation time of ~2000 years, some surface deformation will be driven by large spatial-scale loading changes over longer (millennial-scale) periods interacting with the lower mantle (e.g., Argus et al. (2014)).

Fig. 8 shows the measured horizontal velocity at TRVE (black arrow in Fig. 8) after application of the plate rotation correction. The FOS1 and WLCH horizontal vectors are small and the observation uncertainties were not small enough to separate the various models. In addition to the observed horizontal velocity at TRVE we also plot the predicted horizontal velocity at this location due to decadal viscoelastic deformation (using 345 different Earth models; black points in Fig. 8). Some black points fall inside the observation 2σ (95% confidence interval) uncertainty ellipse but relate to Earth models with the UMV < 9×10^{18} Pa s and the LT < 60 km, which have been already ruled out as shown in Fig. 7a. If we instead applied the ITRF2008 plate rotation model (Altamimi et al., 2011), the observed GPS rates at TRVE would rotate anticlockwise, further away from the model predictions. It is possible that this misfit between

observed and predicted horizontal velocities could be explained by signal related to ice mass loss further offshore during deglaciation.

To explore the potential contribution to present-day deformation from millennial-scale GIA, which includes the response to mass loss from across the whole of Marguerite Bay, each of the 345 decadal-scale viscoelastic model predictions were summed with each of the millennial-scale GIA predictions (colored dots in Fig. 8). We take care not to over-interpret these summed predictions given the different rheological frameworks employed in the different decadal-scale and millennial-scale models. While some models which include millennial-scale GIA move the predictions away from the observation, some are closer and indeed a few points are now located inside the uncertainty ellipse of the observed motion. The closest points (in dark green) use the W12 3D model (S-dry-10 mm). Considering the sensitivity to changes in the decadal-scale Earth model only, those predictions inside the error ellipse are largely insensitive to LT changes (bottom-left inset in Fig. 8), but prefer an UMV ranging from 7×10^{18} Pa s to 3×10^{20} Pa s (bottom-right inset in Fig. 8).

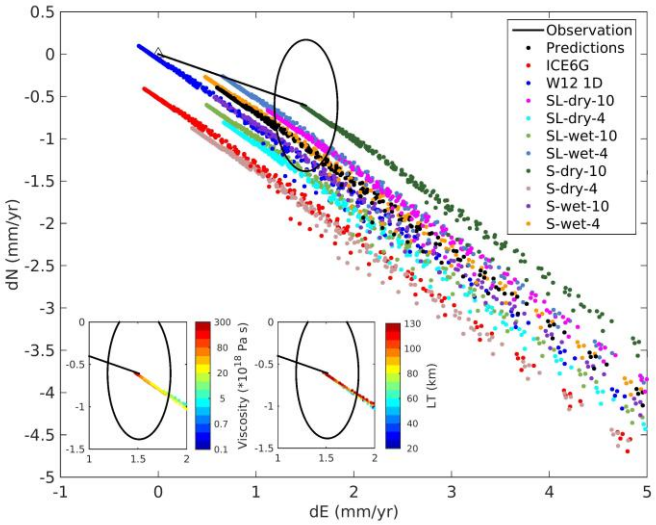

Figure 8. Observed and predicted horizontal rates at TRVE. The black arrow and ellipse indicate the observed GPS horizontal velocity after plate rotation correction and the 2σ uncertainty (σ_N and σ_E in Table 1), respectively. The black points are modelled horizontal velocities due to post-1966 viscoelastic deformation, as detailed in this study (one dot per 345

different model realizations). The colored points are modelled horizontal velocities calculated by summing the predicted post-1966 horizontal velocities from this study (black points) and the post-LGM deformation rates from various millennial-scale GIA models. The two inset panels show the lithospheric thickness and upper mantle viscosity of various models after removing the post-LGM deformation rates using W12 3D (S-dry-10 mm).

Taking into account GPS velocity uncertainties and the uncertainty in modelling plate tectonics and viscoelastic deformation, we are unable to identify a unique set of preferred Earth models via the analysis of horizontal velocities. However, we do find that post-1966 deformation alone cannot explain the observed horizontal velocity at TRVE, and conclude that there must be a contribution from pre-1966 mass loss within Marguerite Bay. In general, our horizontal rates provide a less definitive lower bound on UMV than the vertical rates, but we once again find that the UMV in this region is very likely greater than that found in the northern AP.

6 Discussion

A previous study has calculated ice elevation change rates for Fleming Glacier by comparing data from 2004 and 2008 (Wendt et al., 2010). Our study extends this analysis to span 1966-2015. Our quantification of total lowering since 1966 demonstrates dynamic mass loss sustained over 50 years, indicating that this glacier is likely still far from achieving a new equilibrium. The Fleming Glacier system represents one of the best-quantified examples of long-term change of an Antarctic glacier system following the retreat/collapse of its ice shelf (although we note that ice shelf retreat has been episodic rather than instantaneous, meaning several perturbations to back-stresses have possibly occurred). Little is known of the bathymetry in front of the present-day glacier, and hence it is not known if this historic change is related to unstable grounding line retreat across a reverse sloping bed or not (Schoof, 2007). Underscoring the sustained loss is the sharp increase in the rate of ice surface-lowering at the ice shelf front after 2008 (-6.25$\pm$0.20 m/yr) to a values more than two times that of the 2002-2008 rate (-2.77$\pm$0.89 m/yr), which is consistent with the observed ice velocity increases between 2008 and 2015. This post-2008 lowering is 4 times the multi-decadal average during

1966-2008 (1.5 m/yr), highlighting the magnitude of the dynamic response of the feeding glaciers to the recent disappearance of the ice shelf. We note that these ice elevation change rates could have been higher for a period of time within 2002-2008 or 1966-2008 but the average during these periods is lower than 2008-2015.

Thinning of grounded ice unloads the solid Earth and induces a viscoelastic response. Our quantification of mass change since the ice shelf breakup provides a relatively unusual opportunity to constrain viscous Earth rheology; GIA modelling usually includes uncertainties in both ice history and earth structure, and strong trade-offs between the two are typically present (e.g., Fig.4 in Argus et al. (2014)). In contrast, while uncertainties exist in the earliest part of our ice history, our findings remain robust to different assumptions in that we require at least moderate upper mantle viscosities ($> 2\times10^{19}$ Pa s) in all cases, with little sensitivity to LT. Our preferred dm/dt model suggests that this region is underlain by upper mantle with a similar viscosity ($> 1\times10^{20}$ Pa s; Fig. 7a) to that found for all of Palmer Land (Wolstencroft et al., 2015a). The lack of detailed ice history prior to ice shelf retreat and the short-duration GPS observations are the primary reasons that we cannot further narrow the range of the best fitting Earth models for this region. Improved accuracy and temporal-spatial coverage of GPS data as well as more late Holocene ice extent constraints are therefore essential.

This UMV is in contrast with that found by Nield et al. (2014) in the northern AP, where preferred upper mantle viscosities are around 1×10^{18} Pa s. Allowing for uncertainties on the Earth models we infer for the WIS region, it seems likely that UMV varies by at least a factor of 10 in just over 500 km, although we note the limitation that we cannot represent such structure within the Earth models used in this study. It remains to be determined how smoothly this change occurs.

Wolstencroft et al. (2015a) suggested that the pattern of GPS-observed uplift in Palmer Land could not be explained by existing GIA models and that ice histories in the south-west Weddell Sea region were in some way incorrect – either needing greater ice loss since the LGM or more localized loss during the late Holocene and a moderate-to-low mantle viscosity ($1\text{-}3\times10^{20}$ Pa s).

Our new finding that the TRVE horizontal velocity points away from Marguerite Bay rather than Fleming Glacier is suggestive of a continued response to ice load changes associated with grounding line retreat from a substantially more advanced position within Marguerite Bay. This is in agreement with our findings based on vertical uplift rates and confirms that late Holocene or earlier mass load changes play an important role in defining the solid Earth response of this region. Evidence suggests that initial grounding line retreat occurred within Marguerite Trough at ~14 cal ka BP (Ó Cofaigh et al., 2014) and continued until 9.2-9.6 ka BP (Bentley et al., 2011; Simkins et al., 2013), but little is known of the mid-to-late Holocene ice history of the region.

There is evidence for relative sea-level (RSL) fall in the Marguerite Bay region between ~5.5-7.3 ka BP and 2.5 ka BP, initially at a rate of 3.3 mm/yr, and then at a rate of ~1.4 mm/yr after 2.5 ka BP (Simkins et al., 2013). Given that global deglaciation had largely ended by this period and hence far-field drivers of sea level change were small, we assume that the late-Holocene RSL fall is dominated by local vertical land motion. The solid Earth implications of this sustained uplift depend on the extent to which local ice load changes occurred after 9.2 ka BP, which is not known. An early termination of deglaciation combined with our finding of relatively high mantle viscosity is compatible with this observation, but this is not the only plausible scenario and further Holocene ice loading data are required.

Finally, Nield et al. (2012) investigated the magnitude of solid Earth subsidence associated with accumulation increases in the southern AP between 1855 to 2010, for a range of Earth models. When they used an Earth model that is consistent with our analysis (a thick lithosphere of 71 km and a UMV of 1×10^{20} Pa s), they predicted a present-day subsidence rate of up to 3.2 mm/yr, although we note that their GIA model resolution is not ideal for high resolution studies. We have not considered their loading change in this study because our observation of changes in some way overlap with those reconstructed by the ice sheet model output used by Nield et al. (2012) and hence there is a danger of double-counting. Repeating this modelling effort is a substantial undertaking beyond the scope of the present study. Nonetheless, regional subsidence

over the past 150 years or so makes it plausible that the vertical background rates shown in Fig. 7a could be negative (i.e., uplift prior to the 1850s, then subsidence over 1850-1966), which would bring about a downward revision to our estimated lower bound on upper mantle viscosity.

7 Conclusion

We provide a 50-year quantification of ice elevation changes of glaciers feeding the WIS, associated with the retreat and collapse of this ice shelf. We then use this quantification in conjunction with viscoelastic modelling to provide constraints on viscous Earth rheology in this region.

Comparing DEMs derived from historical aerial photography from 1966 and a satellite-derived DEM from 2008, we identify more than 60 m of ice surface lowering over this time. High-resolution elevation data over 2002 to 2014 in the Fleming Glacier system reveals a changing temporal response of the feeding glaciers with no sign of abatement in glacier thinning. Indeed, thinning rates from 2008-2015 were substantially greater than rates averaged over 1966-2008 and 2002-2008. The increased dynamic thinning in this region may be associated with grounding line retreat or the intrusion of warm Circumpolar Deep Water or mid-depth oceanic warming, perhaps combination with the presence of a possible retrograde bed (Cook et al., 2016; Wouters et al., 2015). The glaciers feeding the WIS are yet to reach a new equilibrium some 50 years after ice shelf retreat commenced.

Using a new high-resolution ice unloading dataset from 1966 to 2015, we simulated solid Earth deformation at three GPS sites. Comparison between the GPS observations and the model predictions revealed a higher viscosity Earth rheology in the southern AP than previously reported in the northern AP (Nield et al., 2014), suggesting a north-south gradient in viscosity, which changes by at least an order of magnitude over 500 km. We find horizontal velocities that, after removal of plate rotation and recent viscoelastic effects, point away from Marguerite Bay. This is suggestive of a continued response to Holocene deglaciation and hence provides further evidence of a relatively strong upper mantle compared with the northern AP where a near-instantaneous viscous response has been observed.

The specific viscoelastic properties of the southern AP still remain to be identified quantitatively, but our analysis establishes an approximate lower bound. Improved Holocene ice loading history, ongoing glacier loading changes, and long-term and high-accuracy GPS time series will help resolve the remaining ambiguity in GIA modelling in this region.

Acknowledgements

CZ is a recipient of an Australian Government Research Training Program Scholarship. MAK is a recipient of an Australian Research Council Future Fellowship (project number FT110100207). PLW is a recipient of a NERC Independent Research Fellowship (NE/K009958/1). The work was partially supported by Australian Research Council Special Research Initiative for Antarctic Gateway Partnership (Project ID SR140300001) and NERC grant NE/F01452X/1. IceBridge ATM and LVIS data used in this paper were all acquired by NASA's Operation IceBridge Project. The 1966 aerial photography was provided by USGS via the Polar Geospatial Center. We thank Etienne Berthier for assistance with the SPOT DEM and British Antarctic Survey engineers for maintaining and downloading the GPS sites. SPOT 5 images and DEMs were provided by the International Polar Year SPIRIT project (Korona et al., 2009), funded by the French Space Agency (CNES). This work is based on data services provided by the UNAVCO Facility with support from the National Science Foundation (NSF) and National Aeronautics and Space Administration (NASA) under NSF Cooperative Agreement No. EAR-0735156. VE-CL0V3RS was developed by V.R.B and A.B in a self-funded project. We thank NASA JPL for making GIPSY available, Richard Peltier for making their model outputs available, and Alex Gardner for making pre-publication velocities available.

Reference

Altamimi, Z., Collilieux, X., Métivier, L., 2011. ITRF2008: an improved solution of the international terrestrial reference frame. Journal of Geodesy 85, 457-473.

Argus, D.F., Peltier, W., Drummond, R., Moore, A.W., 2014. The Antarctica component of postglacial rebound model ICE-6G_C (VM5a) based on GPS positioning, exposure age dating of ice thicknesses, and relative sea level histories. Geophysical Journal International 198, 537-563.

Barletta, V.R., Ferrari, C., Diolaiuti, G., Carnielli, T., Sabadini, R., Smiraglia, C., 2006. Glacier shrinkage and modeled uplift of the Alps. Geophysical research letters 33.

Bentley, M.J., Johnson, J.S., Hodgson, D.A., Dunai, T., Freeman, S.P.H.T., Ó Cofaigh, C., 2011. Rapid deglaciation of Marguerite Bay, western Antarctic Peninsula in the Early Holocene. Quaternary Science Reviews 30, 3338-3349.

Cook, A.J., Fox, A.J., Vaughan, D.G., Ferrigno, J.G., 2005. Retreating Glacier Fronts on the Antarctic Peninsula over the Past Half-Century. Science 308, 541-544.

Cook, A.J., Holland, P.R., Meredith, M.P., Murray, T., Luckman, A., Vaughan, D.G., 2016. Ocean forcing of glacier retreat in the western Antarctic Peninsula. Science 353, 283-286.

Cook, A.J., Murray, T., Luckman, A., Vaughan, D.E., Barrand, N.E., 2012. A new 100-m Digital Elevation Model of the Antarctic Peninsula derived from ASTER Global DEM: methods and accuracy assessment. Earth System Science Data 4, 129-142.

Cook, A.J., Vaughan, D.G., 2010. Overview of areal changes of the ice shelves on the Antarctic Peninsula over the past 50 years. The Cryosphere 4, 77-98.

Doake, C.S.M., 1975. Bottom sliding of a glacier measured from the surface. Nature 257, 780-782.

Doake, C.S.M., Vaughan, D.G., 1991. Breakup of Wordie Ice Shelf, Antarctica. Glaciers-ocean-atmosphere interactions. Proc. symposium, St. Petersburg, 1990, 161-165.

Dziewonski, A.M., Anderson, D.L., 1981. Preliminary reference Earth model. Physics of the Earth and Planetary Interiors 25, 297-356.

Gardner, A.S., Moholdt, G., Scambos, T., Fahnstock, M., Ligtenberg, S., van den Broeke, M., Nilsson, J., 2017. Increased West Antarctic ice discharge and East Antarctic stability over the last seven years. The Cryosphere Discuss. 2017, 1-39.

Gunter, B.C., Didova, O., Riva, R.E.M., Ligtenberg, S.R.M., Lenaerts, J.T.M., King, M.A., Van den Broeke, M.R., Urban, T., 2014. Empirical estimation of present-day Antarctic glacial isostatic adjustment and ice mass change. The Cryosphere 8, 743-760.
Ivins, E.R., James, T.S., Wahr, J., O. Schrama, E.J., Landerer, F.W., Simon, K.M., 2013. Antarctic contribution to sea level rise observed by GRACE with improved GIA correction. Journal of Geophysical Research: Solid Earth 118, 3126-3141.
Ivins, E.R., Raymond, C.A., James, T.S., 2000. The influence of 5000 year-old and younger glacial mass variability on present-day crustal rebound in the Antarctic Peninsula. Earth, planets and space 52, 1023-1029.
King, M.A., 2013. Progress in modelling and observing Antarctic glacial isostatic adjustment. Astronomy & Geophysics 54, 4.33-34.38.
King, M.A., Santamaría-Gómez, A., 2016a. Ongoing deformation of Antarctica following recent Great Earthquakes. Geophysical Research Letters 43, 1918-1927.
King, M.A., Whitehouse, P.L., van der Wal, W., 2016b. Incomplete separability of Antarctic plate rotation from glacial isostatic adjustment deformation within geodetic observations. Geophysical Journal International 204, 324-330.
Korona, J., Berthier, E., Bernard, M., Rémy, F., Thouvenot, E., 2009. SPIRIT. SPOT 5 stereoscopic survey of Polar Ice: Reference Images and Topographies during the fourth International Polar Year (2007–2009). ISPRS Journal of Photogrammetry and Remote Sensing 64, 204-212.
Krabill, W.B., 2014, updated 2016. IceBridge ATM L2 Icessn Elevation, Slope, and Roughness. Version 2. . NASA DAAC at the National Snow and Ice Data Center., Boulder, CO, USA.
McMillan, M., Shepherd, A., Sundal, A., Briggs, K., Muir, A., Ridout, A., Hogg, A., Wingham, D., 2014. Increased ice losses from Antarctica detected by CryoSat-2. Geophysical Research Letters 41, 2014GL060111.
Nield, G.A., Barletta, V.R., Bordoni, A., King, M.A., Whitehouse, P.L., Clarke, P.J., Domack, E., Scambos, T.A., Berthier, E., 2014. Rapid bedrock uplift in the Antarctic Peninsula explained by viscoelastic response to recent ice unloading. Earth and Planetary Science Letters 397, 32-41.
Nield, G.A., Whitehouse, P.L., King, M.A., Clarke, P.J., Bentley, M.J., 2012. Increased ice loading in the Antarctic Peninsula since the 1850s and its effect on glacial isostatic adjustment. Geophysical Research Letters 39.
Ó Cofaigh, C., Davies, B.J., Livingstone, S.J., Smith, J.A., Johnson, J.S., Hocking, E.P., Hodgson, D.A., Anderson, J.B., Bentley, M.J., Canals, M., Domack, E., Dowdeswell, J.A., Evans, J., Glasser, N.F., Hillenbrand, C.-D., Larter, R.D., Roberts, S.J., Simms, A.R., 2014. Reconstruction of ice-sheet changes in the Antarctic Peninsula since the Last Glacial Maximum. Quaternary Science Reviews 100, 87-110.
Peltier, W., 2004. Global glacial isostasy and the surface of the ice-age Earth: the ICE-5G (VM2) model and GRACE. Annu. Rev. Earth Planet. Sci. 32, 111-149.
Peltier, W., Argus, D., Drummond, R., 2015. Space geodesy constrains ice age terminal deglaciation: The global ICE‐6G_C (VM5a) model. Journal of Geophysical Research: Solid Earth 120, 450-487.
Petrov, L., 2015. The international mass loading service. International Association of Geodesy Symposia 146.
Rignot, E., Casassa, G., Gogineni, P., Krabill, W., Rivera, A.u., Thomas, R., 2004. Accelerated ice discharge from the Antarctic Peninsula following the collapse of Larsen B ice shelf. Geophysical Research Letters 31.
Rignot, E., Casassa, G., Gogineni, S., Kanagaratnam, P., Krabill, W., Pritchard, H., Rivera, A., Thomas, R., Turner, J., Vaughan, D., 2005. Recent ice loss from the Fleming and other glaciers, Wordie Bay, West Antarctic Peninsula. Geophysical Research Letters 32.
Rignot, E., Mouginot, J., Scheuchl, B., 2011a. Antarctic grounding line mapping from differential satellite radar interferometry. Geophysical Research Letters 38, L10504.
Rignot, E., Mouginot, J., Scheuchl, B., 2011b. Ice Flow of the Antarctic Ice Sheet. Science 333, 1427-1430.
Santamaría-Gómez, A., Mémin, A., 2015. Geodetic secular velocity errors due to interannual surface loading deformation. Geophysical Journal International 202, 763-767.
Scambos, T.A., Hulbe, C., Fahnestock, M., Bohlander, J., 2000. The link between climate warming and break-up of ice shelves in the Antarctic Peninsula. Journal of Glaciology 46, 516-530.
Schoof, C., 2007. Ice sheet grounding line dynamics: Steady states, stability, and hysteresis. Journal of Geophysical Research: Earth Surface 112, n/a-n/a.
Seehaus, T.C., Marinsek, S., Skvarca, P., van Wessem, J.M., Reijmer, C.H., Seco, J.L., Braun, M.H., 2016. Dynamic Response of Sjögren Inlet Glaciers, Antarctic Peninsula, to Ice Shelf Breakup Derived from Multi-Mission Remote Sensing Time Series. Frontiers in Earth Science 4.

Simkins, L.M., Simms, A.R., DeWitt, R., 2013. Relative sea-level history of Marguerite Bay, Antarctic Peninsula derived from optically stimulated luminescence-dated beach cobbles. Quaternary Science Reviews 77, 141-155.
Thomas, I.D., King, M.A., Bentley, M.J., Whitehouse, P.L., Penna, N.T., Williams, S.D., Riva, R.E., Lavallee, D.A., Clarke, P.J., King, E.C., 2011. Widespread low rates of Antarctic glacial isostatic adjustment revealed by GPS observations. Geophysical Research Letters 38.
Vaughan, D.G., 1993. Implications of the break-up of Wordie Ice Shelf, Antarctica for sea level. Antarctic Science 5, 403-408.
Wendt, J., Rivera, A., Wendt, A., Bown, F., Zamora, R., Casassa, G., Bravo, C., 2010. Recent ice-surface-elevation changes of Fleming Glacier in response to the removal of the Wordie Ice Shelf, Antarctic Peninsula. Annals of Glaciology 51, 97-102.
Whitehouse, P.L., Bentley, M.J., Le Brocq, A.M., 2012b. A deglacial model for Antarctica: geological constraints and glaciological modelling as a basis for a new model of Antarctic glacial isostatic adjustment. Quaternary Science Reviews 32, 1-24.
Whitehouse, P.L., Bentley, M.J., Milne, G.A., King, M.A., Thomas, I.D., 2012a. A new glacial isostatic adjustment model for Antarctica: calibrated and tested using observations of relative sea-level change and present-day uplift rates. Geophysical Journal International 190, 1464-1482.
Williams, S.D.P., 2008. CATS: GPS coordinate time series analysis software. GPS Solutions 12, 147-153.
Wolstencroft, M., King, M.A., Whitehouse, P.L., Bentley, M.J., Nield, G.A., King, E.C., McMillan, M., Shepherd, A., Barletta, V., Bordoni, A., Riva, R.E.M., Didova, O., Gunter, B.C., 2015b. Uplift rates from a new high-density GPS network in Palmer Land indicate significant late Holocene ice loss in the southwestern Weddell Sea. Geophysical Journal International 203, 737-754.
Wouters, B., Martin-Español, A., Helm, V., Flament, T., van Wessem, J.M., Ligtenberg, S.R.M., van den Broeke, M.R., Bamber, J.L., 2015. Dynamic thinning of glaciers on the Southern Antarctic Peninsula. Science 348, 899-903.
Zwally, H., SCHUTZ, R., BENTLEY, C., BUFTON, J., HERRING, T., MINSTER, J., SPINHIRNE, J., THOMAS, R., 2014. GLAS/ICESat L2 Antarctic and Greenland Ice Sheet Altimetry Data Version 34. NASA National Snow and Ice Data Center Distributed Active Archive Center, Boulder, Colorado USA. .